# Molecular spintronics using single-molecule magnets under irradiation

Kieran Hymas and Alessandro Soncini*
*School of Chemistry, University of Melbourne, Parkville, Victoria 3010, Australia*

(Received 21 May 2018; revised manuscript received 6 May 2019; published 10 June 2019)

We theoretically investigate a single-molecule magnet (SMM) grafted to a quantum dot in contact with metallic leads and interacting with a resonant electromagnetic radiation. We explore both the explicit time-dependent behavior and the steady-state current-voltage characteristics of the device when the source lead is ferromagnetic. At zero-bias voltage, a net current is pumped through the device with the source spin current being reversed and amplified in the drain lead; this effect also persists for nonzero bias. We explain this effect in terms of spin transitions in the nanomagnet induced by the resonant radiation followed by their subsequent relaxation via spin-asymmetric charge-transfer processes. We demonstrate that the same effects are recovered in the time-averaged current when the device interacts with pulsed resonant radiation. Moreover, within the pulsed irradiation regime, appropriate choices of pulse length and wait times are shown here to allow the detection of coherent Rabi oscillations of the SMM spin states, via time-averaged spin current measurements.

DOI: 10.1103/PhysRevB.99.245404

## I. INTRODUCTION

Single-molecule magnets (SMMs) are magnetically anisotropic inorganic complexes with large spin moments that display a slow relaxation of the magnetization below a given blocking temperature [1]. When grafted to graphene quantum point contacts or carbon nanotubes, single-molecule magnets have been shown to impart highly anisotropic magnetoconductance hysteresis fingerprints on local electric currents, providing compelling evidence for the existence of an exchange interaction between the giant spin of the SMM and the spin of conduction electrons of the carbon nanostructure [2,3] or phthalocyaninato quantum dots in the case of $TbPc_2$ break junction devices [4,5]. SMMs have been studied in the context of molecular spintronics [6] and show potential as molecular memory units [7] and spin valves [3,8] that may eventually form the foundations of complex spintronic technologies or even more ambitiously, quantum computers.

Recent spin-polarized scanning tunneling microscopy (STM) studies of quantum magnets on surfaces have demonstrated that polarized spin currents can influence and even flip the nanomagnet's spin moment via a spin-transfer torque effect [9,10]. This effect could be used to read or write bits of information to single nanomagnets in spintronics devices. A crucial challenge in the development of molecular quantum spintronics consists of injecting a spin current into a SMM-based device. To date, a spintronics experiment with this format has not yet been realized. A feasible strategy to achieve coupling between a spin current and the quantum spin states of a single-molecule magnet is to graft SMMs onto the surface of a graphene quantum point contact since (i) efficient spin injection in graphene has already been achieved [11,12] and (ii) coupling between SMMs and a graphene quantum dot device has been demonstrated [2].

In this paper we propose and theoretically study a molecular spintronics setup based on a SMM device under resonant irradiation. The aim is to perturb the populations of SMM spin states by inducing simple coherent spin dynamics behavior in the SMM and assess its influence on the spin current flowing through a device via the aforementioned exchange interaction, so that the spin current effectively measures the dynamics of the SMM spin states under irradiation. In SMM-based transport experiments, a sweeping magnetic field is often used in this spirit to probe the incoherent dynamics related to the slow relaxation of the nanomagnet [2,3,13] but here, by using resonant electromagnetic radiation, we are able to study also the coherent oscillatory dynamics of the magnetic subsystem and its interplay with the dissipative dynamics of the leads.

While the spectroscopy of nanomagnets in the bulk phase is relatively commonplace, addressing single (or few) molecules in a spintronic device with radiation is not at all trivial. Recently, STM tips have been employed in this vein to induce atomically localized time-dependent modulations to the crystal field of magnetic atoms adsorbed to a MgO/Ag(001) substrate [14]. Another approach to achieve coherent transitions within a SMM device was demonstrated by Thiele *et al.* [5] whereby the nuclear spin states of a single $TbPc_2$ molecule in a molecular break junction were coupled to resonant microwave signals via the hyperfine Stark effect. While the experimental details of inducing resonant coherent transitions in a nanomagnet spintronics device are intricate and system specific, a radiation-magnetic dipole coupling is archetypal of more general coupling schemes (discussed in Appendix A) that may be utilized in an experimental nanomagnet spintronics setup. In this paper we focus on this simple regime of radiation-dipole coupling in order to illustrate the interesting phenomena that can arise from a nanomagnet spintronic device subject to a resonant, time-dependent perturbation.

We contribute to the already extensive nanomagnet-based spintronics literature [15–22] by considering a SMM configuration with the potential to work as a spin pump and

*asoncini@unimelb.edu.au

 

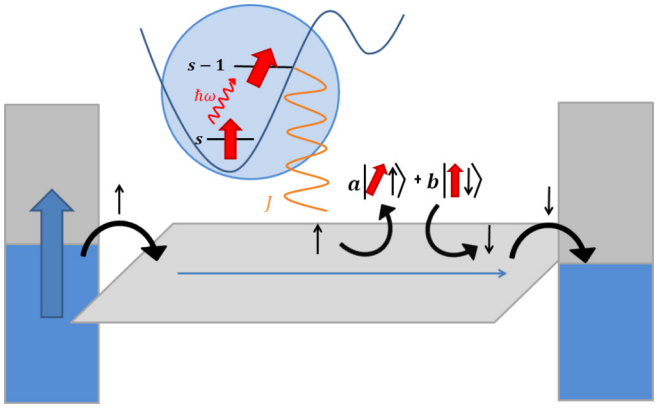


FIG. 1. A schematic representation of electron transport from a ferromagnetic lead through a quantum dot that is antiferromagnetically coupled to a SMM subject to resonant radiation. Energy is supplied to the system to tilt the giant spin of the SMM (thick, red) allowing a spin-majority electron to charge the device from the ferromagnetic source. On relaxation, the SMM aligns against the longitudinal field reversing the spin of the conduction electron as it is emitted to the nonmagnetic drain.

spin switch. Although noncollinear magnetic molecules have been previously presented as efficient spin-switching devices [23,24], the possibility of inducing spin current switching is presented here via a more general SMM system (i.e., without invoking specific noncollinear spin configurations). Finally, we discuss the possibility of reading out Rabi oscillations between spin states via time-averaged spin-current measurements, a result already observed in experiment between the nuclear spin states of a $TbPc_2$ molecule, in which case, however, the device also required a sweeping magnetic field [5].

In Sec. II we present a model describing the operation of our SMM-based spintronic device under irradiation utilizing the density matrix formalism. In Sec. III we show results from our model when both continuous and pulsed radiation are applied and discuss the underlying mechanism that leads to pumping, switching, and amplification of the spin current. Finally, in Sec. IV we recapitulate and make concluding remarks.

## II. THEORETICAL MODEL

### A. Model Hamiltonian

We consider a device (Fig. 1) consisting of a SMM grafted to a quantum dot that is weakly coupled to two metallic leads. We include an interaction with a static longitudinal magnetic field and a gate electrode. At sufficiently low temperatures, we assume that the device operates in the Coulomb blockade regime such that charging and discharging to and from the dot occurs sequentially. We suppose that the onsite Coulomb repulsion between electrons on the dot is large enough to exclude doubly charged states from participating in transport through the device. We also include a coupling between the total spin of the device and the magnetic component of an applied radiation.

The total Hamiltonian for the device reads as

$$H(t) = H_L + H_S + V(t) + H_T, \tag{1}$$

where

$$H_L = \sum_{\alpha k\sigma} (\epsilon_{\alpha k\sigma} - \mu_\alpha) a^\dagger_{\alpha k\sigma} a_{\alpha k\sigma} \tag{2}$$

is the isolated source and drain Hamiltonian, in which $a^{(\dagger)}_{\alpha k\sigma}$ destroys (creates) an electron in lead $\alpha$ with wave vector $\boldsymbol{k}$, spin $\sigma$, and energy $\epsilon_{\alpha k\sigma}$. Here, $\mu_\alpha$ corresponds to the chemical potential of electrons in the Fermi level of lead $\alpha$ which is often modulated in experiment by the application of an antisymmetric bias voltage $V_b$ such that $\mu_L = V_b/2$ and $\mu_R = -V_b/2$. The system Hamiltonian is

$$H_S = -DS_z^2 + \sum_\sigma (\epsilon - eV_g) c^\dagger_\sigma c_\sigma + \mu_B B_z (g_1 S_z + g_2 s_z) - J\boldsymbol{S}\cdot\boldsymbol{s}, \tag{3}$$

where $\boldsymbol{S} = (S_x, S_y, S_z)$ is the SMM spin operator, $c^{(\dagger)}_\sigma$ annihilates (creates) an electron on the dot with spin $\sigma$, and $\boldsymbol{s} = (s_x, s_y, s_z)$ is the spin operator for the aforementioned radical. $D$ is the uniaxial anisotropy characterizing the zero-field splitting of the SMM spin states, $g_1$ and $g_2$ are the $g$ factors for the SMM and the dot, respectively, $\mu_B$ is the Bohr magneton, $B_z$ is the amplitude of a static longitudinal magnetic field, $\epsilon$ is the one-electron dot-orbital energy, $V_g$ is the magnitude of an applied gate voltage, and $J$ is the exchange coupling between the SMM and an electron on the dot. The tunneling Hamiltonian is simply

$$H_T = \sum_{\alpha k\sigma} T^*_\alpha a^\dagger_{\alpha k\sigma} c_\sigma + T_\alpha c^\dagger_\sigma a_{\alpha k\sigma}, \tag{4}$$

where $T_\alpha$ are the tunneling amplitudes for charging and discharging events between lead $\alpha$ and the dot; we neglect the possibility of direct tunneling between source and drain leads.

We discuss here the simplest radiation-dipole coupling regime that can induce magnetic dipole-allowed resonant transitions in the ground spin multiplet of the nanomagnet. We approximate the magnetic component of radiation propagating along the easy axis of the nanomagnet as a rotating transverse magnetic field that couples to the giant spin of the SMM by a Zeeman interaction. We take the field to be rotating clockwise with a frequency $\omega$ in the plane perpendicular to the easy axis of the SMM so that

$$V(t) = g_1 \mu_B B_\perp [S_x \cos(\omega t) - S_y \sin(\omega t)], \tag{5}$$

where $B_\perp$ is the amplitude of the magnetic component of the radiation.

After noting that the $z$ component of the total spin operator (defined by $\boldsymbol{S}^t = \boldsymbol{S} + \boldsymbol{s}$) commutes with $H_S$, it is convenient to enumerate the energy eigenstates of $H_S$ with the eigenvalues of $S^t_z$. We use a notation where $|n, m\rangle$ denotes an electronic state of the SMM-dot hybrid with a total spin projection $m$ and with $n$ electrons occupying the lowest unoccupied molecular orbital (LUMO) of the dot. The energy eigenstates of the neutral and charged systems are $|0, m\rangle \equiv |m\rangle \otimes |vac\rangle$ and $|1, m\rangle^\pm \equiv \mathbb{A}^\pm_m |m + 1/2\rangle \otimes |\downarrow\rangle + \mathbb{B}^\pm_m |m - 1/2\rangle \otimes |\uparrow\rangle$, respectively; the fully polarized states are simply $|1, s + 1/2\rangle \equiv$

$|s\rangle \otimes |\uparrow\rangle$ and $|1, -s-1/2\rangle \equiv |-s\rangle \otimes |\downarrow\rangle$. The coefficients $\mathbb{A}_m^{\pm}$ and $\mathbb{B}_m^{\pm}$ are of the form

$$\mathbb{A}_m^{\pm} = \pm\frac{|J|}{J}\frac{\sqrt{2\Delta\epsilon(m) \mp [(2D-J)m - \mu_B B_z \delta g]}}{2\sqrt{\Delta\epsilon(m)}},$$

$$\mathbb{B}_m^{\pm} = \frac{|J|\sqrt{s(s+1)-m^2+1/4}}{2\sqrt{\Delta\epsilon(m)}\sqrt{2\Delta\epsilon(m) \mp [(2D-J)m - \mu_B B_z \delta g]}} \quad (6)$$

with $\Delta\epsilon(m) = [(\mu_B B_z \delta g/2)^2 + \mu_B B_z \delta g(2D-J)m/2 + D(D-J)m^2 + (J/4)^2(2s+1)^2]^{1/2}$ and $\delta g = g_1 - g_2$. The energies of the electronic states of the SMM-dot hybrid are $E(0,m) = -Dm^2 - g_1\mu_B m B_z$ and $E(1,m)^{\pm} = \epsilon - V_g + J/4 - D(m^2+1/4) - g_1\mu_B m B_z \pm \Delta\epsilon(m)$. The energies of the fully polarized charged states are given by $E(1, \pm s \pm 1/2)^{+}$ when $2D - J \geqslant 0$ and $E(1, \pm s \pm 1/2)^{-}$ otherwise.

From here we shall be concerned with the $2D - J > 0$ regime in which the charged ground states are the antiferromagnetic $|1, \pm s \mp 1/2\rangle^{-}$ states. Note that the exchange part of the Hamiltonian in Eq. (3) mixes states of the SMM-dot hybrid that conserve the axial projection of the total spin of the device. Thus, in the antiferromagnetic coupling regime the charged ground states are linear combinations of SMM spin states; this is a crucial condition for the operation of the device as discussed later. We choose $B_z < 0$ to lift the degeneracy of both neutral and charged spectra but are careful not to choose $|B_z|$ so large that the ferromagnetic $|1, s+1/2\rangle$ state becomes the new ground state of the charged system. Finally, we impose a level degeneracy condition between the $|0, s\rangle$ and $|1, s-1/2\rangle^{-}$ states by choosing a suitable gate voltage $V_g$ so that $|E(0,s) - E(1, s-1/2)^{-}| = 0$.

### B. Master equation in a time-dependent resonant field and stationary current

The reduced density matrix describing the electronic spin states of the SMM-dot hybrid is defined by $\rho(t) = \mathrm{Tr}_L\{\rho^{\mathrm{tot}}(t)\}$ where $\rho^{\mathrm{tot}}(t)$ is the density matrix for the entire device and $\mathrm{Tr}_L\{\dots\}$ denotes a trace over states in the leads. A system of differential equations for $\rho(t)$ is obtained within the Born-Markov approximation by making standard manipulations [25] to the Von Neumann equation, however, neglecting the effect of $V(t)$ in the unperturbed propagators used to transform the equations of motion of the density matrix into the interaction picture. It is self-consistent to neglect the effect of the radiation in the definition of the interaction picture provided that the transitions caused by $V(t)$ are much slower than the decay of correlations in the leads induced by $H_T$ [26]. After retaining only the secular terms in the resultant master equation (the validity of which is investigated in Appendix B), the evolution of a reduced density matrix element is governed by

$$\dot{\rho}_{mm'} = \frac{-i}{\hbar}[H_S + V(t), \rho]_{mm'} + \delta_{mm'}\sum_l W^{l\to m}\rho_l - \gamma_{mm'}\rho_{mm'}, \quad (7)$$

where $\rho_{mm'} = \langle n, m|\rho(t)|n, m'\rangle$ is a matrix element between eigenstates of $H_S$ (we do not consider coherences between states from different charge spaces and so unambiguously drop the index $n$ in $\rho_{mm'}$), $\gamma_{mm'} = \frac{1}{2}\sum_l W^{m\to l} + W^{m'\to l}$ is the total decoherence rate, and $W^{l\to m} = \sum_{\alpha\sigma} W^{l\to m}_{\alpha\sigma}$ are rates of charging/discharging (summed over leads and spin) from a state $|n, l\rangle$ to a state $|n', m\rangle$ given by [18]

$$W^{l\to m}_{\alpha\sigma} = \frac{\Gamma_\alpha(1+2\sigma P_\alpha)}{2\hbar}\begin{cases} \left|c^{n\to n+1}_{\sigma,ml}\right|^2 f_\alpha(\Delta_{ml}), \\ \left|c^{n\to n-1}_{\sigma,ml}\right|^2 [1 - f_\alpha(\Delta_{lm})], \end{cases} \quad (8)$$

where the upper case applies for charging transitions ($n' = n+1$) and the lower case applies for discharging transitions ($n' = n-1$). In the expression above, $f_\alpha(\Delta) = \{1 + \exp[\beta(\Delta \mp V_b/2)]\}^{-1}$ is the Fermi-Dirac distribution for electrons in lead $\alpha$, the argument $\Delta$ is the energy difference between the relevant charged and neutral states, $-(+)V_b$ corresponds to the applied bias voltage at the source (drain) lead, $\beta = 1/k_B T$ where $T$ is temperature and $k_B$ is Boltzmann's constant, $\Gamma_\alpha$ is the coupling strength between lead $\alpha$ and the SMM-dot hybrid, and $P_\alpha$ is the spin polarization inherent to lead $\alpha$. Finally, $c^{n\to n+1}_{\sigma,ml} = \langle n', m|c^{\dagger}_{\sigma}|n, l\rangle$ and $c^{n\to n-1}_{\sigma,ml} = \langle n', m|c_\sigma|n, l\rangle$ are the charging and discharging transition amplitudes, respectively. Note that $W^{l\to m}$ is only nonzero when the number of conduction electrons is changed by one and the total spin of the SMM-dot hybrid is changed by one-half, i.e., $|n' - n| = 1$ and $|l - m| = 1/2$.

In the Coulomb blockade regime, at low temperatures and bias voltages, only the $|0, s\rangle$, $|0, s-1\rangle$, and $|1, s-1/2\rangle^{-}$ states make significant contributions to the current flowing through the device and so we focus only on the evolution of these states. Since the $|1, s-1/2\rangle^{+}$ state will not participate in transport, we will from now on unambiguously refer to $|1, s-1/2\rangle^{-}$ as $|1, s-1/2\rangle$ in order to ease notation. Due to the presence of $V(t)$ inside the commutator in Eq. (7) we obtain rate equations with an explicit time dependence in the coefficients of the density matrix elements. This explicit time dependence can be eliminated [26] by changing to the rotating reference frame $|n, m\rangle_R = e^{im\omega t}|n, m\rangle$ so that $\rho_{mm'} = e^{i\omega(m-m')t}\rho^R_{mm'}$. In the rotating frame, the relevant rate equations take the form

$$\begin{aligned}
\dot{\rho}^R_s &= \frac{\sqrt{2s}g_1\mu_B B_\perp}{\hbar}\mathrm{Im}\{\rho^R_{s-1,s}\} \\
&\quad + W^{s-1/2\to s}\rho^R_{s-1/2} - W^{s\to s-1/2}\rho^R_s, \\
\dot{\rho}^R_{s-1} &= \frac{\sqrt{2s}g_1\mu_B B_\perp}{\hbar}\mathrm{Im}\{\rho^R_{s,s-1}\} \\
&\quad + W^{s-1/2\to s-1}\rho^R_{s-1/2} - W^{s-1\to s-1/2}\rho^R_{s-1}, \\
\dot{\rho}^R_{s-1/2} &= W^{s\to s-1/2}\rho^R_s + W^{s-1\to s-1/2}\rho^R_{s-1} \\
&\quad - (W^{s-1/2\to s} + W^{s-1/2\to s-1})\rho^R_{s-1/2}, \\
\dot{\rho}^R_{s-1,s} &= \frac{i\sqrt{2s}g_1\mu_B B_\perp}{2\hbar}(\rho^R_{s-1} - \rho^R_s) \\
&\quad - i(\Delta_{s-1,s} - \omega)\rho^R_{s-1,s} - \gamma_{s-1,s}\rho^R_{s-1,s}, \\
\dot{\rho}^R_{s,s-1} &= \frac{i\sqrt{2s}g_1\mu_B B_\perp}{2\hbar}(\rho^R_s - \rho^R_{s-1}) \\
&\quad - i(\Delta_{s,s-1} + \omega)\rho^R_{s,s-1} - \gamma_{s,s-1}\rho^R_{s,s-1},
\end{aligned} \quad (9)$$

where $\Delta_{s-1,s} = [E(0,s-1) - E(0,s)]/\hbar$. We approximate the coherences in the rotating frame by setting $\dot{\rho}^R_{s-1,s} = \dot{\rho}^R_{s,s-1} = 0$ so that by inverting the last two equations in Eq. (9) we obtain expressions for $\rho^R_{s-1,s}$ and $\rho^R_{s,s-1}$. The imaginary parts of the coherences are Lorentzian line shapes multiplied by the difference in the nonequilibrium populations of the two states involved in the coherent superposition, and are given by

$$\mathrm{Im}\{\rho^R_{s-1,s}\} = \frac{\sqrt{2s}g_1\mu_B B_\perp}{2\hbar}\frac{\gamma_{s-1,s}(\rho^R_{s-1} - \rho^R_s)}{(\Delta_{s-1,s}-\omega)^2 + \gamma^2_{s-1,s}} \tag{10}$$

with $\mathrm{Im}\{\rho^R_{s,s-1}\} = -\mathrm{Im}\{\rho^R_{s-1,s}\}$. Note that the Lorentzian line shapes appearing in Eq. (10) are broadened by the total decoherence rate $\gamma_{s-1,s}$, and peaked at $\omega = \Delta_{s-1,s}$, thus defining the resonance condition for the dissipative system. After inserting the imaginary part of the coherences into the top two expressions in Eq. (9) we obtain a $3 \times 3$ system of differential equations containing only the diagonal components of the reduced density matrix in the rotating reference frame. To explore the stationary current limit, we invoke a further steady-state approximation and solve for the long-time behavior of the diagonal components of the density matrix. The solutions may be transformed back into the rest frame trivially as the diagonal components of the density matrix do not pick up an explicit time dependence when shifting between frames.

We calculate the total current and the spin current at lead $\alpha$ with

$$\begin{aligned} I^{(\alpha)}_t &= \pm e(I_{\alpha\uparrow} + I_{\alpha\downarrow}), \\ I^{(\alpha)}_s &= \pm e(I_{\alpha\uparrow} - I_{\alpha\downarrow}), \end{aligned} \tag{11}$$

respectively, where the plus (minus) sign is used for the source (drain), $e$ is the elementary charge,

$$\begin{aligned} I_{\alpha\sigma} = {} & W^{s\to s-1/2}_{\alpha\sigma}\rho_s + W^{s-1\to s-1/2}_{\alpha\sigma}\rho_{s-1} \\ & - \left(W^{s-1/2\to s}_{\alpha\sigma} + W^{s-1/2\to s-1}_{\alpha\sigma}\right)\rho_{s-1/2}, \end{aligned} \tag{12}$$

and $\rho_s$, $\rho_{s-1}$, $\rho_{s-1/2}$ are the rest frame reduced density matrix elements obtained above.

## III. RESULTS AND DISCUSSION

For the purpose of our calculations we have chosen some reasonable parameters describing an easy-axis spin system containing all the necessary properties to behave as a SMM with $s = 6$, $D = 0.02$ meV, and $J = -0.06$ meV. We further choose $B_z = -0.2$ T, $B_\perp = 2 \times 10^{-3}$ T, $\Gamma_S = \Gamma_D = 10^{-3}$ meV, $T = 10$ mK, and $\omega = \Delta_{s-1,s} = 3.5 \times 10^{11}$ s$^{-1}$. $V_g$ is always chosen to impose a level degeneracy condition between the ground states of the neutral and charged manifolds rendering $\epsilon$ an arbitrary parameter. We consider a system with $g_1 = g_2 = 2$ but note that the implications of our model are not restricted by this choice. Variation of $g_1$ will change the position of the level degeneracy; this can be compensated for by adjusting $V_g$. With this choice of parameters, the resulting energy levels of the neutral and singly charged states of the device have the structure presented in Fig. 2. It is particularly important to note that due to the antiferromagnetic coupling assumed here, the lowest-lying exchange coupled state is $|1, s-1/2\rangle$ while the ferromagnetic state is thermally inaccessible for charge transport. We consider the case of an idealized spintronics experiment in which the source lead is ferromagnetic and spin injection is 100% effective ($P_S = 1$) while the drain remains nonmagnetic ($P_D = 0$).

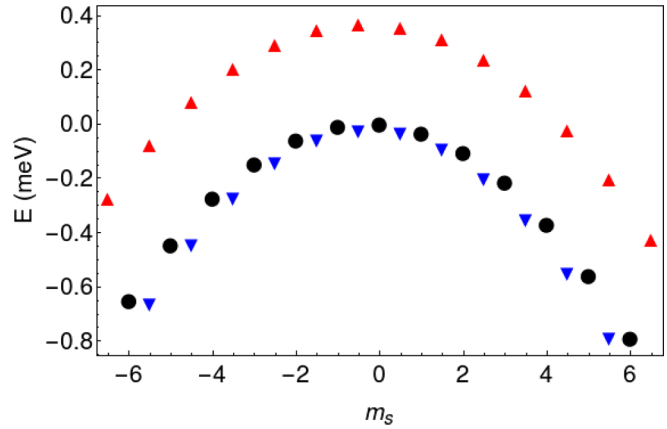


FIG. 2. Energy levels of the SMM-dot hybrid described by the Hamiltonian given in Eq. (3) calculated using parameters chosen above. The neutral states are represented by black dots and the plus (minus) charged states by upward-facing (red) [downward-facing (blue)] triangles.

### A. Continuous radiation

In order to investigate the time-dependent coherent dynamics of the magnetic system induced by the resonant radiation, we first performed brute force numerical integration of Eq. (7). In addition, numerical integration of Eq. (7) provides a means to assess the robustness of the approximations leading to the analytic steady-state solutions obtained for Eq. (9). Figure 3 shows the time evolution of the relevant diagonal elements of $\rho(t)$ obtained at $V_b = 0$ when the SMM hybrid is initially prepared in the $|0, s\rangle$ state. The radiation induces damped Rabi oscillations between $|0, s\rangle$ and $|0, s-1\rangle$ that quickly decay to a steady state due to decoherence introduced by the incoherent charge-transfer process between the the leads and the open quantum system. We find that the long-time behavior of these solutions agrees with the analytical solutions

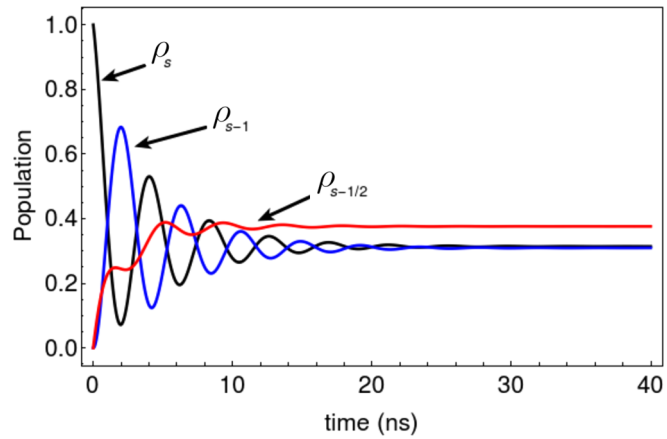


FIG. 3. Time evolution of the $\rho_s$, $\rho_{s-1/2}$, and $\rho_{s-1}$ density matrix elements obtained by numerical integration of Eq. (7) at $V_b = 0$ with a ferromagnetic source.

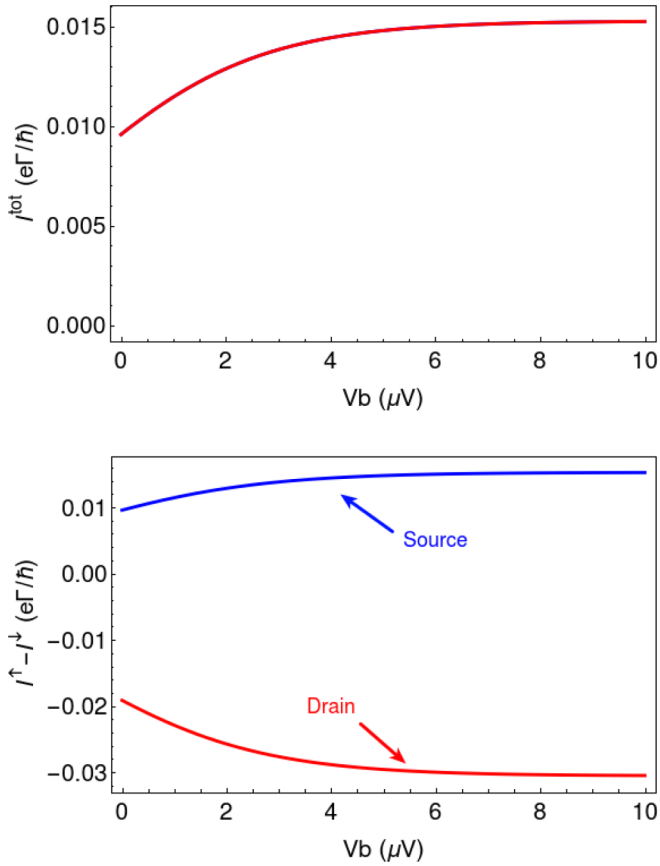


FIG. 4. The stationary charge current (top) and spin currents at source and drain (bottom) flowing through the device as a function of applied bias voltage.

obtained from our treatment of the master equation above, therefore corroborating the steady-state approximations leading to Eq. (10). The rate of population transfer between $|0, s\rangle$ and $|0, s-1\rangle$ at steady state is related to the imaginary part of the off-diagonal matrix element given in Eq. (10) and is thus maximal when $\omega = \Delta_{s-1,s}$. The energy supplied to the device via continuous irradiation drives a population imbalance in the neutral manifold leading to the manifestation of several interesting steady-state transport effects.

Figure 4 shows the stationary charge and spin currents as a function of applied bias voltage flowing through the device. A net current is pumped through the device at zero-bias voltage with the majority-spin current injected from the ferromagnetic source being completely reversed and amplified at the drain. When the SMM is prepared in the $|0, s\rangle$ ground state via an external magnetic field along the easy axis but is not irradiated, then charging from the source can not occur as the ferromagnetic reduced state $|1, s+1/2\rangle$ of the device is thermally inaccessible for transport (see Fig. 2). One may view this configuration as the high-resistance state of a molecular spin valve where the single-molecule magnet acts as a spin analyzer. When energy is supplied to the system by resonant electromagnetic radiation (see Fig. 1 for a schematic), then the giant spin of the SMM is tilted via transfer of population to the excited $|0, s-1\rangle$ state. A spin-majority electron may now charge the device owing to the nonzero amplitude $\langle 1, s-1/2|c_{\uparrow}^{\dagger}|0, s-1\rangle$ between the $|0, s-1\rangle$ and $|1, s-1/2\rangle = \mathbb{A}^{-}_{s-1/2}|s\rangle \otimes |\downarrow\rangle + \mathbb{B}^{-}_{s-1/2} \otimes |s-1\rangle|\uparrow\rangle$ states. The only nonzero discharging process that can take place from $|1, s-1/2\rangle$ is one in which the SMM is returned to its maximal spin ground state $|s\rangle$, and therefore only discharging of spin-minority electrons is possible, due to the coherent superposition structure of $|1, s-1/2\rangle$; crucially, this can occur *only at the drain* owing to the fully spin-polarized character of the ferromagnetic source lead. Thus, even at zero-bias voltage, a spin-switched current is pumped through the device due to energy supplied via the resonant radiation and the spin-asymmetric charge-transfer processes at the ferromagnetic source and nonmagnetic drain. We note that at low temperatures the $|0, s-1\rangle$ state lies outside of the conduction window provided that $V_b < 2\Delta_{s-1,s-1/2} = D(2s-1) - g_1\mu_B B_z$. As a consequence, when the $|0, s-1\rangle$ is populated as a result of the resonant electromagnetic radiation, the device may also be charged by electrons from the drain that also undergo a spin reversal before being emitted back to the drain. Although this process does not contribute to the net charge current flowing through the device, it does provide an additional contribution to the negative spin current at the drain resulting in an amplification of the drain spin current. These effects persist for nonzero bias voltage provided that the bias is not so large as to activate the ferromagnetic $|1, s+1/2\rangle$ charged state or to include $|0, s-1\rangle$ in the conduction window. While the charge pumping described here is reminiscent of the photon-assisted tunneling already observed in quantum dots [27,28], we stress that in this setup it is the SMM that absorbs the radiation in order to overcome the current blockade rather than the conduction electron.

### B. Pulsed radiation

The continuous irradiation model described in the previous section may present practical challenges in attaining constant temperature of the system due to heat dissipation involved by the absorption process. Thus, we also explore a perhaps more easily realizable experimental setup, investigating the spintronics problem under pulsed radiation. Accordingly, we define a timescale $t_{p+w} = t_p + t_w$ corresponding to a single pulse-wait sequence. During the interval $t \in [0, t_p]$ the radiation is switched on and $V(t)$ is given by Eq. (5), whereas in the interval $t \in [t_p, t_{p+w}]$ the radiation is switched off and $V(t) = 0$; this sequence is repeated for multiples of $t_{p+w}$. We calculate the average current through the device by numerical integration of the master equation followed by averaging of the time-dependent current over an arbitrary number of pulse-wait sequences occurring after the initial pulse. For clarity, we define the time average of a function $f(t)$ over the time domain $T = \{t \in \mathbb{R} \mid t_a \leqslant t \leqslant t_b\}$ by

$$\langle f \rangle_T = \frac{1}{t_b - t_a} \int_{t_a}^{t_b} f(t)\, dt. \tag{13}$$

We focus on the case when $V_b = 0$ and investigate the dependence of the time-averaged current on the pulse and wait times $t_p$ and $t_w$, respectively.

Figure 5 shows the time-averaged current flowing through the device at zero bias for values of $t_p$ and $t_w$. Even here we obtain a finite time-averaged charge current for all values of $t_p \neq 0$ which tends toward saturation as $t_p \to \infty$ and

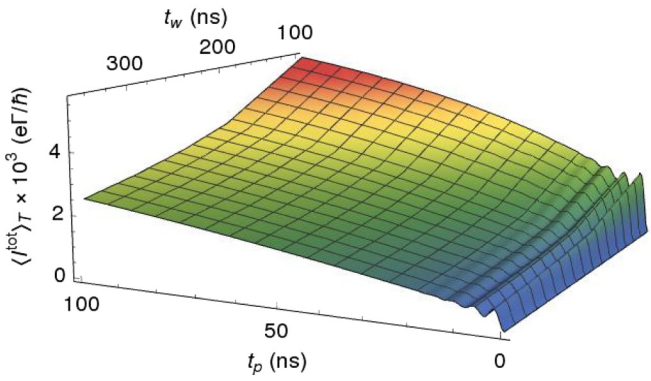


FIG. 5. The time-averaged charge current flowing through the device at $V_b = 0$ as a function of various pulse times $t_p$ and wait times $t_w$.

manifests an oscillatory behavior as $t_p \to 0$. By increasing the wait time in-between pulses, we see that the average charge current per $t_{p+w}$ cycle diminishes and tends to zero for $t_w \to \infty$.

As noted previously, the resonant radiation causes damped Rabi oscillations between elements of the density matrix (see Fig. 3) which is consequently reflected in the time-dependent current. When $t_p$ is shorter than the decay of the damped oscillations, $\langle I^{\rm tot}\rangle_T$ provides piecewise measurements of the time evolution of the Rabi oscillations between $|0, s\rangle$ and $|0, s-1\rangle$. Conversely, when $t_p$ is longer than the decay of the damped Rabi oscillations, the system is able to reach a *quasi*-steady-state limit (as in the continuous irradiation model) within the pulse phase of each $t_{p+w}$ cycle and, therefore, the oscillations are averaged out in $\langle I^{\rm tot}\rangle_T$. During wait sequences [where $V(t) = 0$] the coherences in Eq. (7) become completely decoupled from the diagonal elements of the density matrix and the master equation becomes completely soluble up until the next pulse. Specializing to the $3 \times 3$ system discussed above, we solve $\dot{\rho} = \mathcal{M}\rho$ over $t_p \leqslant t \leqslant t_{p+w}$ where $\rho = (\rho_s, \rho_{s-1}, \rho_{s-1/2})^T$ and $\mathcal{M}$ is the time-independent rate matrix describing charging and discharging processes between the dot and the leads. A great deal of simplification can be made when $V_b = 0$ as $W^{s-1/2\to s-1} \approx 0$ and $W^{s\to s-1/2} = W^{s-1/2\to s}$, leading one to discover the eigenvalues of $\mathcal{M}$ as $\{0, -2W^{s\to s-1/2}, -W^{s-1\to s-1/2}\}$. Recalling that the long-time limit of the system in the absence of resonant radiation leads to a blockage of current we see that, regardless of $t_p$, for $t_w > \max(-2W^{s\to s-1/2}, -W^{s-1\to s-1/2})$ no current flows through the device resulting in a diminishing value of $\langle I^{\rm tot}\rangle_T$ as $t_w \to \infty$.

Although in this section we have focused only on the time-averaged charge current in the pulsed radiation regime, we note that the time-averaged spin currents (not shown) are also switched and amplified at the drain as in the continuous radiation model. The behavior of the time-averaged spin currents as functions of $t_p$ and $t_w$ is mirrored in the discussion above and so we omit it here. For the device to function optimally, $t_p$ and $t_w$ should be chosen such that the $|0, s-1\rangle$ state is sufficiently populated on each $t_{p+w}$ cycle and also such that heat acquired from the resonant radiation diffuses away from the SMM before the next pulse. We do not investigate the added complexity of heat diffusion in this paper.

### C. Candidate nanomagnets for the device

In the model presented above, we have made no mention of the specific SMM that should be used in the junction as we predict the pumping, switching, and amplification effects described above to be achievable with any nanomagnet that is well described by the Hamiltonian given in Eq. (3). In a practical setting, however, the choice of SMM is far from arbitrary as the frequency of radiation required for the $m = s \to s-1$ transition may also couple to vibrational modes in the molecule or contribute to other undesirable interactions. $Fe_4$-based nanomagnets could be prime candidates for the device proposed above as their magnetic properties are retained following surface deposition [29] and have been shown to be robust under successive oxidation and reduction in three terminal devices [30,31]. A first-principles theoretical study of an $Fe_4$ nanomagnet attached to metallic leads has furthermore indicated that the magnetic properties of $Fe_4$ are likely to be preserved in such a junction and may enjoy a modest increase in uniaxial anisotropy on reduction [32]. The aforementioned theoretical work by Nossa *et al.* partially corroborates the assumption made by Burzuri *et al.* [31] in that $Fe_4$ acquires a $S = \frac{9}{2}$ ground state on reduction, implying an antiferromagnetic coupling between the giant spin of the magnet and the radical. In addition, the gap between the ground and excited states on graphene has been reported $\sim$1 $cm^{-1}$ which could be probed with microwave radiation [33,34]. Octanuclear Fe(III) nanomagnets are also good candidates for the device since the gap $\Delta_{s-1,s} \sim 4$ $cm^{-1}$ is also amenable to microwave radiation. In fact, the $m = s \to s-1$ transition in $Fe_8$ SMM crystals has already been probed with pulsed microwave radiation in previous studies [35–39]. The required radiation-induced transition in $Mn_{12}$ could also be achieved with microwave radiation as it has been reported to possess a $\Delta_{s-1,s}$ of $\sim$9 $cm^{-1}$ [40]. $Cr_7M$ ($M$ = Cd, Mn, Ni) molecular wheels may also be excellent candidates for our device given their stability on surface deposition [41,42] and under microwave radiation [43,44].

## IV. CONCLUSION

We have proposed a model for electron transport through a SMM nanostructure under irradiation in the Coulomb blockade regime. We demonstrated that a spin current is pumped through the device at zero-bias voltage when coupled to a ferromagnetic source as a result of radiation-induced transitions in the SMM followed by spin-asymmetric discharging at the source and drain leads. In addition to this spin-pumping effect, we find that the spin-polarized current pumped from the source is reversed and amplified at the drain even when $V_b \neq 0$. We also investigated the behavior of the device under pulsed irradiation and discussed the time-averaged current as a function of pulse length and wait time. We find that for long enough pulse lengths and short wait times the stationary current results are recovered. Interestingly, however, for short pulse lengths and long wait times we also find that the proposed device can be used to measure coherent Rabi oscillations between the SMM spin states, which could offer an as yet unexplored strategy to integrate SMM-based spin qubits into spintronics circuits.

## ACKNOWLEDGMENTS

K.H. acknowledges the support from the Australian Government Research Training Program Scholarship. A.S. acknowledges support from the Australian Research Council, Future Fellowship No. FT180100519. We thank A. Candini and M. Affronte for their suggestions regarding the pulsed radiation model.


## APPENDIX A: ALTERNATE RESONANT PERTURBATION COUPLING SCHEMES

Throughout this paper we have discussed the spin-transport dynamics imparted to a SMM-dot hybrid device with a specific radiation-dipole coupling scheme [see Eq. (5)]. A more general coupling between the magnetic states of the SMM and a resonant coherent perturbation can be achieved with the Hamiltonian

$$V_N(t) = \nu[S_+^N e^{i\omega t} + S_-^N e^{-i\omega t}], \tag{A1}$$

where $N \in \mathbb{N}$ and $\nu$ is some constant specific to the applied resonant perturbation in a given experimental setup. Note that Eq. (5) is recovered from Eq. (A1) when $N = 1$ and $\nu = g_1\mu_B B_\perp$. To investigate the consequences on the spin-transport dynamics of the device when the ground spin state $|0, s\rangle$ is coherently and resonantly coupled to an excited spin state $|0, s-N\rangle$ with $N > 1$, we proceeded as in the main text and developed a master equation for the reduced density matrix elements akin to Eq. (7), but with the substitution $V(t) \mapsto V_N(t)$. Using the parameters from Sec. III with $\omega = \Delta_{s-N,s}$, we computed the zero-bias steady-state spin currents at the ferromagnetic source and nonmagnetic drain electrodes for several values of $N$ and nanomagnet spin quantum numbers $s$.

If $N > s$, the resonant perturbation will induce population transfer over the nanomagnet anisotropy barrier thus quenching the spin pumping, switching, and amplification effects described above. Multiple excitations caused by $V_N(t)$, while occurring on the slowest timescales can, in the steady-state limit, also result in population transfer over the barrier even when $N < s$; these processes are suppressed, however, with increasing $s$ or $D$. Provided that $N$ is not too large with respect to the barrier height, Fig. 6 demonstrates that coupling the ground state $|0, s\rangle$ to excited states with axial spin projections less than $s-1$ with a resonant perturbation can still give rise to the current pumping, switching, and amplification effects described in the main text. As $N$ is increased, these effects are augmented owing to the multistep charging/discharging cascade that is required to relax the nanomagnet from the excited state $|0, s-N\rangle$ to the ground state $|0, s\rangle$. For example, consider a resonant perturbation that couples $|0, s\rangle$ and $|0, s-2\rangle$: after each excitation from the ground state to $|0, s-2\rangle$ relaxation proceeds via the charging/discharging cascade $|0, s-2\rangle \to |1, s-3/2\rangle^- \to |0, s-1\rangle \to |1, s-1/2\rangle^- \to |0, s\rangle$. In this example, two electrons much sequentially charge and discharge from the device both with their individual spin moments switched hence leading to a larger spin current than observed in the $N = 1$ case. Finally, we note that for the nanomagnet spintronics setup outlined here with a resonant perturbation $V_{N>1}(t)$, calculation of the steady-state spin currents can be reduced to that of the effective three-state model described in the main text with only the lead-dot coupling $\Gamma_\alpha$ renormalized to account for the multistep charging/discharging cascade.

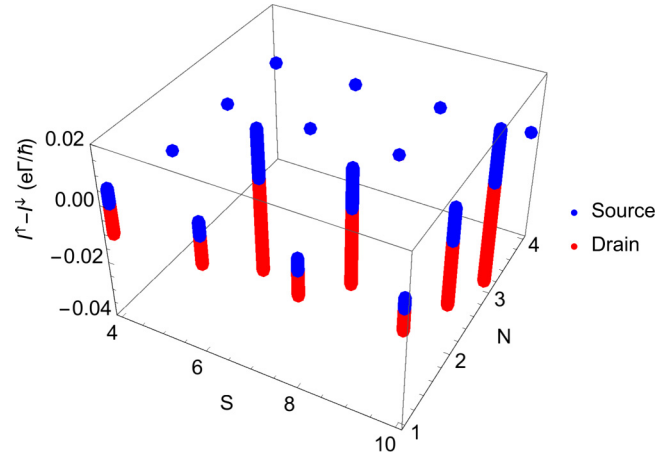


FIG. 6. Zero-bias steady-state spin currents at the source and drain electrodes for SMM devices with various spin quantum numbers $s$ and resonant perturbations $V_N(t)$.

## APPENDIX B: NONSECULAR RATE EQUATION

In order to confirm the validity of the secular approximation leading to Eq. (7), we performed a numerical integration of the full nonsecular quantum master equation. The evolution of a reduced density matrix element is

$$\dot{\rho}_{mm'} = \frac{-i}{\hbar}[H_S + V(t), \rho]_{mm'} + (\mathcal{R}\rho)_{mm'}, \tag{B1}$$

where $\mathcal{R}$ controls the full nonsecular dynamics of the device owing to the dissipative effects from coupling to the leads and is given explicitly by

$$\begin{aligned}(\mathcal{R}\rho)_{mm'} = \sum_{\alpha}^{S,D}\sum_{\sigma}^{\uparrow\downarrow}\frac{\Gamma_\alpha(1+2\sigma P_\alpha)}{4\hbar}\Bigg\{&\sum_{kl}^{n+1} c_{\sigma,ml}^{n+1\to n}\rho_{lk}c_{\sigma,km'}^{n\to n+1}[2 - f_\alpha(\Delta_{lm}) - f_\alpha(\Delta_{km'})] \\ &+ \sum_{kl}^{n-1} c_{\sigma,ml}^{n-1\to n}\rho_{lk}c_{\sigma,km'}^{n\to n-1}[f_\alpha(\Delta_{ml}) + f_\alpha(\Delta_{m'k})] - \sum_{k}^{n}\sum_{l}^{n+1} f_\alpha(\Delta_{lk})\left(c_{\sigma,ml}^{n+1\to n}c_{\sigma,lk}^{n\to n+1}\rho_{km'} + \rho_{mk}c_{\sigma,kl}^{n+1\to n}c_{\sigma,lm'}^{n\to n+1}\right) \\ &- \sum_{k}^{n}\sum_{l}^{n-1}[1 - f_\alpha(\Delta_{kl})]\left(c_{\sigma,ml}^{n-1\to n}c_{\sigma,lk}^{n\to n-1}\rho_{km'} + \rho_{mk}c_{\sigma,kl}^{n-1\to n}c_{\sigma,lm'}^{n\to n-1}\right)\Bigg\}.\end{aligned} \tag{B2}$$

We found the numerical solutions to Eq. (B1) to be indistinguishable from those that result from a quantum rate equation containing only secular terms (Fig. 3). The secular approximation is thus justified for this system as the nonsecular dynamics of the coherences induced by the dissipative effect of the leads occurs on a much faster timescale than the time evolution of the populations $\rho_m$ and as such are canceled out upon integration.


[1] G. Christou, D. Gatteschi, D. N. Hendrickson, and R. Sessoli, Single-molecule magnets, MRS Bull. **25**, 66 (2000).

[2] A. Candini, S. Klyatskaya, M. Ruben, W. Wernsdorfer, and M. Affronte, Graphene spintronic devices with molecular nanomagnets, Nano Lett. **11**, 2634 (2011).

[3] M. Urdampilleta, S. Klyatskaya, J.-P. Cleuziou, M. Ruben, and W. Wernsdorfer, Supramolecular spin valves, Nat. Mater. **10**, 502 (2011).

[4] R. Vincent, S. Klyatskaya, M. Ruben, W. Wernsdorfer, and F. Balestro, Electronic read-out of a single nuclear spin using a molecular spin transistor, Nature (London) **488**, 357 (2012).

[5] S. Thiele, F. Balestro, R. Ballou, S. Klyatskaya, M. Ruben, and W. Wernsdorfer, Electrically driven nuclear spin resonance in single-molecule magnets, Science **344**, 1135 (2014).

[6] L. Bogani and W. Wernsdorfer, Molecular spintronics using single-molecule magnets, Nat. Mater. **7**, 179 (2008).

[7] M. Mannini, F. Pineider, P. Sainctavit, C. Danieli, E. Otero, C. Sciancalepore, A. M. Talarico, M.-A. Arrio, A. Cornia, D. Gatteschi *et al.*, Magnetic memory of a single-molecule quantum magnet wired to a gold surface, Nat. Mater. **8**, 194 (2009).

[8] M. Urdampilleta, S. Klayatskaya, M. Ruben, and W. Wernsdorfer, Magnetic interaction between a radical spin and a single-molecule magnet in a molecular spin-valve, ACS Nano **9**, 4458 (2015).

[9] A. A. Khajetoorians, B. Baxevanis, C. Hübner, T. Schlenk, S. Krause, T. O. Wehling, S. Lounis, A. Lichtenstein, D. Pfannkuche, J. Wiebe *et al.*, Current-driven spin dynamics of artificially constructed quantum magnets, Science **339**, 55 (2013).

[10] S. Krause, L. Berbil-Bautista, G. Herzog, M. Bode, and R. Wiesendanger, Current-induced magnetization switching with a spin-polarized scanning tunneling microscope, Science **317**, 1537 (2007).

[11] W. Han, K. Pi, K. M. McCreary, Y. Li, J. J. I. Wong, A. G. Swartz, and R. K. Kawakami, Tunneling Spin Injection into Single Layer Graphene, Phys. Rev. Lett. **105**, 167202 (2010).

[12] M. Ohishi, M. Shiraishi, R. Nouchi, T. Nozaki, T. Shinjo, and Y. Suzuki, Spin injection into a graphene thin film at room temperature, Jpn. J. Appl. Phys. **46**, L605 (2007).

[13] F. Troiani, C. Godfrin, S. Thiele, F. Balestro, W. Wernsdorfer, S. Klyatskaya, M. Ruben, and M. Affronte, Landau-Zener Transition in a Continuously Measured Single-Molecule Spin Transistor, Phys. Rev. Lett. **118**, 257701 (2017).

[14] S. Baumann, W. Paul, T. Choi, C. P. Lutz, A. Ardavan, and A. J. Heinrich, Electron paramagnetic resonance of individual atoms on a surface, Science **350**, 417 (2015).

[15] C. Timm and F. Elste, Spin amplification, reading, and writing in transport through anisotropic magnetic molecules, Phys. Rev. B **73**, 235304 (2006).

[16] C. Romeike, M. R. Wegewijs, W. Hofstetter, and H. Schoeller, Quantum-Tunneling-Induced Kondo Effect in Single Molecular Magnets, Phys. Rev. Lett. **96**, 196601 (2006).

[17] M. R. Wegewijs, C. Romeike, H. Schoeller, and W. Hofstetter, Magneto-transport through single-molecule magnets: Kondo-peaks, zero-bias dips, molecular symmetry and Berry's phase, New J. Phys. **9**, 344 (2007).

[18] M. Misiorny and J. Barnaś, Spin polarized transport through a single-molecule magnet: Current-induced magnetic switching, Phys. Rev. B **76**, 054448 (2007).

[19] F. Delgado, J. J. Palacios, and J. Fernández-Rossier, Spin-Transfer Torque on a Single Magnetic Adatom, Phys. Rev. Lett. **104**, 026601 (2010).

[20] J. W. González, F. Delgado, and J. Fernández-Rossier, Graphene single-electron transistor as a spin sensor for magnetic adsorbates, Phys. Rev. B **87**, 085433 (2013).

[21] A. Hurley, N. Baadji, and S. Sanvito, Spin-flip inelastic electron tunneling spectroscopy in atomic chains, Phys. Rev. B **84**, 035427 (2011).

[22] H. Xie, Q. Wang, B. Chang, H. Jiao, and J.-Q. Liang, Spin current and polarization reversal through a single-molecule magnet with ferromagnetic electrodes, J. Appl. Phys. **111**, 063707 (2012).

[23] J. Crabtree and A. Soncini, Toroidal quantum states in molecular spin-frustrated triangular nanomagnets with weak spin-orbit coupling: Applications to molecular spintronics, Phys. Rev. B **98**, 094417 (2018).

[24] A. Soncini and L. F. Chibotaru, Molecular spintronics using noncollinear magnetic molecules, Phys. Rev. B **81**, 132403 (2010).

[25] K. Blum, *Density Matrix Theory and Applications* (Springer, Berlin, 2012).

[26] H.-A. Engel and D. Loss, Single-spin dynamics and decoherence in a quantum dot via charge transport, Phys. Rev. B **65**, 195321 (2002).

[27] L. P. Kouwenhoven, S. Jauhar, K. McCormick, D. Dixon, P. L. McEuen, Y. V. Nazarov, N. C. vanderVaart, and C. T. Foxon, Photon-assisted tunneling through a quantum dot, Phys. Rev. B **50**, 2019 (1994).

[28] L. P. Kouwenhoven, S. Jauhar, J. Orenstein, P. L. McEuen, Y. Nagamune, J. Motohisa, and H. Sakaki, Observation of Photon-Assisted Tunneling through a Quantum Dot, Phys. Rev. Lett. **73**, 3443 (1994).

[29] A. Cini, M. Mannini, F. Totti, M. Fittipaldi, G. Spina, A. Chumakov, R. Rüffer, A. Cornia, and R. Sessoli, Mössbauer spectroscopy of a monolayer of single molecule magnets, Nat. Commun. **9**, 480 (2018).

[30] A. S. Zyazin, J. W. G. van den Berg, E. A. Osorio, H. S. J. van der Zant, N. P. Konstantinidis, M. Leijnse, M. R. Wegewijs, F. May, W. Hofstetter, and C. Danieli, Electric field controlled magnetic anisotropy in a single molecule, Nano Lett. **10**, 3307 (2010).

[31] E. Burzurí, A. S. Zyazin, A. Cornia, and H. S. J. Van der Zant, Direct Observation of Magnetic Anisotropy in an Individual $Fe_4$ Single-Molecule Magnet, Phys. Rev. Lett. **109**, 147203 (2012).

[32] J. F. Nossa, M. F. Islam, C. M. Canali, and M. R. Pederson, Electric control of a $Fe_4$ single-molecule magnet in a single-electron transistor, Phys. Rev. B **88**, 224423 (2013).

[33] C. Cervetti, A. Rettori, M. G. Pini, A. Cornia, A. Repolles, F. Luis, M. Dressel, S. Rauschenbach, K. Kern, M. Burghard *et al.*, The classical and quantum dynamics of molecular spins on graphene, Nat. Mater. **15**, 164 (2016).

[34] C. Schlegel, J. Van Slageren, M. Manoli, E. K. Brechin, and M. Dressel, Direct Observation of Quantum Coherence in Single-Molecule Magnets, Phys. Rev. Lett. **101**, 147203 (2008).

[35] M. Bal, J. R. Friedman, W. Chen, M. Tuominen, C. Beedle, E. Rumberger, and D. Hendrickson, Radiation-and phonon-bottleneck–induced tunneling in the $Fe_8$ single-molecule magnet, Europhys. Lett. **82**, 17005 (2008).

[36] M. Bal, J. R. Friedman, E. Rumberger, S. Shah, D. Hendrickson, N. Avraham, Y. Myasoedov, H. Shtrikman, and E. Zeldov, Photon-induced magnetization changes in single-molecule magnets, J. Appl. Phys. **99**, 08D103 (2006).

[37] S. Bahr, K. Petukhov, V. Mosser, and W. Wernsdorfer, Pump-Probe Experiments on the Single-Molecule Magnet $Fe_8$: Measurement of Excited Level Lifetimes, Phys. Rev. Lett. **99**, 147205 (2007).

[38] K. Petukhov, S. Bahr, W. Wernsdorfer, A. L. Barra, and V. Mosser, Magnetization dynamics in the single-molecule magnet $Fe_8$ under pulsed microwave irradiation, Phys. Rev. B **75**, 064408 (2007).

[39] L. Sorace, W. Wernsdorfer, C. Thirion, A.-L. Barra, M. Pacchioni, D. Mailly, and B. Barbara, Photon-assisted tunneling in a $Fe_8$ single-molecule magnet, Phys. Rev. B **68**, 220407(R) (2003).

[40] A. L. Barra, D. Gatteschi, and R. Sessoli, High-frequency epr spectra of a molecular nanomagnet: Understanding quantum tunneling of the magnetization, Phys. Rev. B **56**, 8192 (1997).

[41] V. Corradini, R. Biagi, U. Del Pennino, V. De Renzi, A. Gambardella, M. Affronte, C. Muryn, G. Timco, and R. Winpenny, Isolated heterometallic $Cr_7Ni$ rings grafted on Au (111) surface, Inorg. Chem. **46**, 4937 (2007).

[42] A. Ghirri, V. Corradini, C. Cervetti, A. Candini, U. Del Pennino, G. Timco, R. J. Pritchard, C. Muryn, R. Winpenny, and M. Affronte, Deposition of functionalized $Cr_7Ni$ molecular rings on graphite from the liquid phase, Adv. Funct. Mater. **20**, 1552 (2010).

[43] A. Ardavan, O. Rival, J. Morton, S. J. Blundell, A. M. Tyryshkin, G. A. Timco, and R. Winpenny, Will Spin-Relaxation Times in Molecular Magnets Permit Quantum Information Processing? Phys. Rev. Lett. **98**, 057201 (2007).

[44] S. Piligkos, H. Weihe, E. Bill, F. Neese, H. El Mkami, G. M. Smith, D. Collison, G. Rajaraman, G. A. Timco, R. Winpenny *et al.*, EPR spectroscopy of a family of $Cr^{III}{}_7M^{II}$ (M= Cd, Zn, Mn, Ni)"wheels": Studies of isostructural compounds with different spin ground states, Chem. Eur. J. **15**, 3152 (2009).